PTEP

Prog. Theor. Exp. Phys. **2019**, 093G01 (14 pages)
DOI: 10.1093/ptep/ptz098

A compact Paul ion trap for the study of space-charge effects in drift-tube linear accelerators

Hiromi Okamoto*, Kunihiro Kojima, and Kiyokazu Ito

Graduate School of Advanced Sciences of Matter, Hiroshima University, 1-3-1 Kagamiyama, Higashi-Hiroshima 739-8530, Japan
*E-mail: okamoto@sci.hiroshima-u.ac.jp

Received June 11, 2019; Revised July 25, 2019; Accepted August 2, 2019; Published September 26, 2019

Starting from the principle of least action, we derive a general Hamiltonian that describes the collective motion of an intense charged-particle bunch in a drift-tube linear accelerator. The Alvarez-type structure is assumed as an example, but the present theory can readily be extended to other types of conventional linacs. A Hamiltonian formalism of non-neutral plasma in a linear Paul trap is also constructed, which demonstrates clear similarity between the linac system and compact ion-trap system. The physical equivalence between these two dynamical systems can be employed to perform a fundamental design study of high-intensity hadron linacs in a local tabletop environment. For the tabletop experiment on space-charge effects in short proton and heavy-ion bunches, we have designed an ion trap whose overall dimension is less than 10 cm axially and whose aperture size is 1 cm in diameter. The new trap is introduced in the S-POD (Simulator of Particle Orbit Dynamics) apparatus developed at Hiroshima University for "Laboratory Accelerator Physics."

Subject Index G02, G10, G15

1. Introduction

The effect of interparticle Coulomb interaction on beam stability is one of the most essential issues in accelerator physics. It is becoming increasingly important due to the rapid progress of accelerator technologies, which has vastly improved the beam quality.[1] In order to deepen our current understanding of space-charge effects for better machine performance, an entirely new experimental approach was established at Hiroshima University after a decade of effort. The unique tabletop apparatus developed at Hiroshima is called "S-POD" (Simulator of Particle Orbit Dynamics) [1,2]. The idea is based on the isomorphism between two closed sets of equations: one for the collective motion of a relativistic beam propagating through an alternating-gradient (AG) transport channel and the other for the collective motion of a non-neutral plasma confined in a compact ion trap [3,4]. This analogy guarantees that the two systems behave in a dynamically similar way. Making use of S-POD, we have studied various topics including space-charge-driven coherent instabilities, resonance crossing, halo formation, noise-induced effects, etc. [5–12].

Analogous experimental devices have been used for beam-physics purposes at a few other laboratories. Gilson and his co-workers constructed an ion trap named "PTSX" (Paul Trap Simulator Experiment) at Princeton Plasma Physics Laboratory [13–15]. It is based on the same operating

[1] See, e.g., the proceedings of the series of ICFA Advanced Beam Dynamics Workshops on High-Intensity and High-Brightness Hadron Beams, http://www.jacow.org.

principle as S-POD, though the electrode design and overall dimensions of the trap are rather different. "IBEX" (Intense Beam EXperiment) is another tabletop experiment closely following the S-POD setup [16,17]. Sheehy of Oxford University and some accelerator experts at Rutherford Appleton Laboratory are going to use IBEX for intense beam studies, including the modeling of novel non-linear lattices [18].

The accelerator-free approach to beam dynamics has many practical advantages. Needless to say, the plasma-trap systems are far more compact and incomparably cheaper than any large-scale machines. Fundamental parameters such as the betatron tunes and particle density are controllable over a wide range. It is even possible to change the AG lattice configuration without any mechanical modifications to the trap structure. Thanks to the simple nature of the system, the trap experiment has little background noise to complicate the output signals. Since the kinetic energies of trapped particles are very low, we do not have to worry about radio-activation due to particle losses. The concept of "Laboratory Accelerator Physics" based on non-neutral plasma traps offers a promising means for the design study of advanced high-intensity machines.

We have mostly employed the so-called "linear Paul trap" (LPT) in S-POD, paying particular attention to collective effects in the transverse degrees of freedom.[2] The standard LPT structure is basically like a quadrupole mass analyzer [19]. The quadrupole rods of the LPTs used for past S-POD experiments are relatively long, which makes the axial potential well approximately flat over the plasma confinement region. We can then form a long ion bunch typical of hadron rings [4]. In addition, the axial well is kept static to prevent the synchrotron motion from being resonantly driven by the external field. This setup greatly simplifies the collective behavior of the plasma, allowing us to emulate the two-dimensional models often adopted in beam-transport theories and computer simulations. As the understanding of transverse dynamics has been deepened through S-POD data for the last decade or more, we are now ready to take a step forward to explore three-dimensional (3D) effects, especially the interplay of the synchrotron and betatron oscillations in intense short bunches. Such information is vital in the design stage and performance improvement of high-intensity hadron linacs. We consider here the drift-tube linac (DTL) structure [20–25] widely employed for proton and heavy-ion acceleration in relatively low-energy regions where the space charge plays an essential role [26,27].

The paper is organized as follows. In Sect. 2 the Hamiltonian of an intense beam is derived assuming the Alvarez-type DTL. We also derive the Hamiltonian of an intense ion plasma in an LPT to prove that these two many-body systems are approximately equivalent. A typical LPT setup to replicate the DTL is then outlined in Sect. 3, together with the detailed design of the LPT recently introduced in S-POD for forthcoming short-bunch experiments. Finally, a summary of the present work is given in Sect. 4.

2. Hamiltonians

We derive the Hamiltonian H_{DTL} of a charged-particle beam in a DTL and the Hamiltonian H_{LPT} of a non-neutral plasma in an LPT, starting from the principle of least action

$$\delta \int L_t \, dt = 0, \tag{1}$$

[2] Another type of non-neutral plasma trap referred to as the "Penning–Malmberg trap" with multi-ring electrodes can also be used as a tabletop tool for beam-physics experiments [3,7].

where L_t is the Lagrangian using time t as the independent variable. The mass and charge state of particles are denoted, respectively, by m and q. The cylindrical coordinate system is used with the z-axis set either along the design beam line of the DTL or along the LPT axis.

2.1. *Drift tube linac*

Assuming the axisymmetric TM mode ($B_z = 0$) generated by an accelerating structure of period $2\ell_c$, Maxwell's equations give the radio-frequency (rf) electromagnetic fields

$$\begin{cases} E_z = \displaystyle\sum_{n=0}^{\infty} a_n I_0(k_n r) \cos\frac{n\pi z}{\ell_c} \cos\omega t, \\ E_r = \displaystyle\sum_{n=0}^{\infty} \frac{n\pi a_n}{k_n \ell_c} I_1(k_n r) \sin\frac{n\pi z}{\ell_c} \cos\omega t, \\ B_\theta = -\displaystyle\sum_{n=0}^{\infty} \frac{\omega a_n}{k_n c^2} I_1(k_n r) \cos\frac{n\pi z}{\ell_c} \sin\omega t, \end{cases} \tag{2}$$

where I_n is the modified Bessel function of order n, c is the speed of light, ω is the angular rf frequency, a_n is the nth Fourier coefficient, and $k_n^2 = (2\pi/\lambda)^2[(n\lambda/2\ell_c)^2 - 1]$ with λ being the rf wavelength. All the other field components, i.e. E_θ, B_r, and B_z, are zero. When the velocity of the synchronous particle is $\beta_s c$, we have $\ell_c = \beta_s\lambda$ for the Alvarez-type DTL and $\ell_c = \beta_s\lambda/2$ for the Wideröe-type DTL. The following discussion focuses on the Alvarez-type structure, but the extension of the present formalism to other types of DTLs is straightforward.

The rf fields in Eq. (2) can be derived from the vector potential $\boldsymbol{A}^{(\mathrm{rf})}$ with the components

$$\begin{cases} A_z^{(\mathrm{rf})} = -\dfrac{1}{\omega}\displaystyle\sum_{n=0}^{\infty} a_n I_0(k_n r) \cos\frac{n\pi z}{\ell_c} \sin\omega t, \\ A_\theta^{(\mathrm{rf})} = 0, \\ A_r^{(\mathrm{rf})} = -\dfrac{1}{\omega}\displaystyle\sum_{n=0}^{\infty} \frac{n\pi a_n}{k_n \ell_c} I_1(k_n r) \sin\frac{n\pi z}{\ell_c} \sin\omega t. \end{cases} \tag{3}$$

In order to give an approximate expression for the Fourier coefficients, we assume that the axial electric field exists only within every accelerating gap of width g and is uniform at the aperture radius r_0. Writing the gap field as $E_z(r = r_0, z) = E_0\ell_c/g$, where E_0 is constant, we obtain

$$a_0 = \frac{E_0}{I_0(k_0 r_0)}, \quad a_n = \frac{2E_0}{I_0(k_n r_0)} \cdot \frac{\sin(n\pi g/2\ell_c)}{n\pi g/2\ell_c} \quad \text{for } n = 2, 4, 6, \ldots, \tag{4}$$

and $a_n = 0$ for odd harmonic numbers [24,25]. In the Alvarez DTL, the forward traveling wave of $n = 2$ is used for beam acceleration. The contributions from other traveling waves of different phase velocities can be ignored, which enables us to simplify the vector potential to

$$\begin{cases} A_z^{(\mathrm{rf})} = \dfrac{E_0 T}{\omega} I_0(kr) \sin\left(\dfrac{2\pi z}{\ell_c} - \omega t\right), \\ A_r^{(\mathrm{rf})} = -\dfrac{2\pi E_0 T}{\omega k \ell_c} I_1(kr) \cos\left(\dfrac{2\pi z}{\ell_c} - \omega t\right), \end{cases} \tag{5}$$

where $T = \dfrac{1}{I_0(kr_0)} \cdot \dfrac{\sin(\pi g/\beta_s\lambda)}{\pi g/\beta_s\lambda}$ and $k \equiv k_2 = 2\pi/\beta_s\gamma_s\lambda$ with $\gamma_s = 1/\sqrt{1-\beta_s^2}$, the Lorentz factor of the synchronous particle. The total energy of the synchronous particle increases as

$$\frac{dW_s}{dz} = qE_z(r=0, \psi=\psi_s) \approx qE_0 T\cos\psi_s, \tag{6}$$

with the synchronous phase defined by

$$\psi_s = \omega\int^z \frac{dz}{\beta_s c} - \frac{2\pi z}{\ell_c}. \tag{7}$$

For simplicity, ψ_s is assumed to be constant from the entrance to the exit of the DTL.

In beam dynamics, it is most convenient to take the longitudinal coordinate z, instead of time t, as the independent variable. The Lagrangian of a relativistic charged particle moving under the influence of electromagnetic fields can then be written in cylindrical coordinates as

$$L_z \equiv L_t\frac{dt}{dz} = -mc\sqrt{(ct')^2 - 1 - (r')^2 - (r\theta')^2} + q(A_r r' + A_\theta r\theta' + A_z - \phi_{sc}t'), \tag{8}$$

where $\boldsymbol{A} = (A_r, A_\theta, A_z)$ is the total vector potential, and the prime mark stands for differentiation with respect to z. The source of the scalar potential ϕ_{sc} is the particles' charge. The vector potential $\boldsymbol{A}$ comes from the rf accelerating field, beam focusing magnets, and space charge. Only the axial component is necessary to describe the transverse magnetic field, i.e. $\boldsymbol{A}^{(mag)} = (0, 0, A_z^{(mag)})$. If we regard the beam as a uniform axial current, the space-charge-induced vector potential can be approximated by $\boldsymbol{A}^{(sc)} = (0, 0, A_z^{(sc)})$, where $A_z^{(sc)} \approx \beta_s\phi_{sc}/c$. The total vector potential in the axial direction is the sum of three functions, $A_z = A_z^{(rf)} + A_z^{(mag)} + \beta_s\phi_{sc}/c$, while the radial component $A_r = A_r^{(rf)}$ and the azimuthal component $A_\theta = 0$.

The Hamiltonian derived from the Lagrangian L_z is

$$H_{DTL} = -\sqrt{p^2 - (p_r - qA_r^{(rf)})^2 - \frac{p_\theta^2}{r^2}} - q(A_z^{(rf)} + A_z^{(mag)}) - \frac{q\beta_s}{c}\phi_{sc}, \tag{9}$$

where the canonical momenta conjugate to the coordinates (r, θ, t) are denoted by (p_r, p_θ, p_t), and p represents the kinetic momentum given by $p = \sqrt{(p_t + q\phi_{sc})^2/c^2 - m^2c^2}$. For the synchronous particle, we have $p_s \equiv \sqrt{(W_s/c)^2 - m^2c^2} = m\beta_s\gamma_s c$. After expanding the square root in Eq. (9) into a power series under the assumption that p is much greater than the transverse momenta, we retain only low-order terms to obtain

$$\begin{aligned} H_{DTL} \approx & -p + \frac{1}{2p_s}\left[p_r + \frac{2\pi qE_0T}{\omega k\ell_c}I_1(kr)\cos\left(\frac{2\pi z}{\ell_c} - \omega t\right)\right]^2 + \frac{p_\theta^2}{2p_s r^2} \\ & - \frac{qE_0T}{\omega}I_0(kr)\sin\left(\frac{2\pi z}{\ell_c} - \omega t\right) + \frac{qG(z)r^2\cos 2\theta}{2} - \frac{q\beta_s}{c}\phi_{sc}, \end{aligned} \tag{10}$$

where $-G(z)$ is the z-dependent step function representing the field gradient of the quadrupole focusing magnets along the beam line. For later convenience, we transform the canonical variables (t, p_t) to the relative time and energy $(\Delta t, -\Delta W)$ employing the generating function

$$F_1(t, -\Delta W; z) = -(\Delta W + W_s)\left(t - \int^z \frac{dz}{\beta_s c}\right). \tag{11}$$

The transformed Hamiltonian is

$$H_{\rm DTL} \approx \frac{(\Delta W)^2}{2p_{\rm s}(\beta_{\rm s}\gamma_{\rm s}c)^2} + \frac{1}{2p_{\rm s}}\left[p_r + \frac{2\pi qE_0T}{\omega k\ell_{\rm c}} I_1(kr)\cos(\omega\Delta t + \psi_{\rm s})\right]^2 + \frac{p_\theta^2}{2p_{\rm s}r^2} + \frac{qE_0T}{\omega}[I_0(kr)\sin(\omega\Delta t + \psi_{\rm s}) - \omega\Delta t\cos\psi_{\rm s}] + \frac{qG(z)r^2\cos 2\theta}{2} + \frac{q}{\beta_{\rm s}\gamma_{\rm s}^2 c}\phi_{\rm sc}. \quad (12)$$

Assuming the small amplitude oscillations of particles in a bunch, we can approximately write $\sin(\omega\Delta t + \psi_{\rm s}) \approx \omega\Delta t\cos\psi_{\rm s} + \sin\psi_{\rm s}[1 - (\omega\Delta t)^2/2]$ and $\cos(\omega\Delta t + \psi_{\rm s}) \approx \cos\psi_{\rm s} - \omega\Delta t\sin\psi_{\rm s}$. It is also allowed to put $I_0(kr) \approx 1 + (kr)^2/4$ and $I_1(kr) \approx kr/2$ because the radial coordinate r of any particle is usually much less than the cell length $\ell_{\rm c} = \beta_{\rm s}\lambda$, i.e. $kr = 2\pi r/\beta_{\rm s}\gamma_{\rm s}\lambda \ll 1$. Substitution of these approximate relations into Eq. (12) leads to the linearized Hamiltonian

$$H_{\rm DTL} \approx \frac{(\Delta W)^2}{2p_{\rm s}(\beta_{\rm s}\gamma_{\rm s}c)^2} + \frac{1}{2p_{\rm s}}\left(p_r + \frac{\pi qE_0T}{\omega\ell_{\rm c}} r\cos\psi_{\rm s}\right)^2 + \frac{p_\theta^2}{2p_{\rm s}r^2} - \frac{qE_0T\omega\sin\psi_{\rm s}}{2}(\Delta t)^2 + \frac{qE_0T\sin\psi_{\rm s}}{4\omega}(kr)^2 + \frac{qG(z)r^2\cos 2\theta}{2} + \frac{q}{\beta_{\rm s}\gamma_{\rm s}^2 c}\phi_{\rm sc}. \quad (13)$$

The r-dependent term in the bracket (the second term) on the right-hand side brings about a focusing effect in the transverse direction. In fact, introducing the new radial canonical variables $(\hat{r}, \hat{p}_r)$ generated by

$$F_2(r, \hat{p}_r; z) = r\hat{p}_r - \frac{\pi qE_0T}{2\omega\ell_{\rm c}} r^2\cos\psi_{\rm s}, \quad (14)$$

we find

$$H_{\rm DTL} \approx \frac{(\Delta W)^2}{2p_{\rm s}(\beta_{\rm s}\gamma_{\rm s}c)^2} + \frac{1}{2p_{\rm s}}\left[\hat{p}_r^2 + \left(\frac{p_\theta}{r}\right)^2\right] + \frac{p_{\rm s}}{2}\left(\frac{\gamma_{\rm s}\sigma_\parallel}{2\pi}\right)^2(\omega\Delta t)^2 - \frac{p_{\rm s}\sigma_\parallel^2}{4}\left[1 - \left(\frac{\gamma_{\rm s}\sigma_\parallel}{2\pi}\cot\psi_{\rm s}\right)^2\right]\left(\frac{r}{\ell_{\rm c}}\right)^2 + \frac{qG(z)r^2\cos 2\theta}{2} + \frac{q}{\beta_{\rm s}\gamma_{\rm s}^2 c}\phi_{\rm sc}, \quad (15)$$

where $\hat{r}$ has been replaced by r for brevity because $\hat{r} = r$, and $\sigma_\parallel$ is the synchrotron phase advance defined by $\sigma_\parallel^2 = -2\pi q\lambda E_0T\sin\psi_{\rm s}/mc^2\beta_{\rm s}\gamma_{\rm s}^3$ for a negative synchronous phase, i.e. when $\sin\psi_{\rm s} < 0$. While the radial cross term ($\propto rp_r$) in Eq. (13) is removed successfully, a focusing term due to the velocity change in the accelerating gap appears. The contribution from the new term is usually small compared with the familiar rf defocusing term in the relatively low beam-energy range where the Coulomb self-field potential $\phi_{\rm sc}$ plays a particularly important role. Since our primary interest here is the collective phenomena originating from $\phi_{\rm sc}$, we simply ignore the effect of rf acceleration in the following. The Hamiltonian can then be simplified to

$$\tilde{H}_{\rm DTL} = \frac{1}{2}\left[\tilde{p}_r^2 + \left(\frac{\tilde{p}_\theta}{r}\right)^2 + \tilde{p}_z^2\right] + \left[\frac{qG(z)\ell_{\rm c}^2\cos 2\theta}{2p_{\rm s}} - \frac{\sigma_\parallel^2}{4}\right]\left(\frac{r}{\ell_{\rm c}}\right)^2 + \frac{\sigma_\parallel^2}{2}\left(\frac{\Delta z}{\ell_{\rm c}}\right)^2 + \frac{q}{p_{\rm s}\beta_{\rm s}\gamma_{\rm s}^2 c}\phi_{\rm sc}, \quad (16)$$

with the scaled variables

$$\tilde{p} = \frac{\hat{p}_r}{p_s}, \quad \tilde{p}_\theta = \frac{p_\theta}{p_s}, \quad \tilde{p}_z = -\frac{\Delta W}{p_s \beta_s \gamma_s c}, \quad \Delta z = \beta_s \gamma_s c \Delta t, \quad \text{and} \quad \tilde{H}_{\rm DTL} = \frac{H_{\rm DTL}}{p_s}.$$

Similar 3D Hamiltonians can be found in Refs. [28] and [29]. It is worth noting that the axisymmetric term ($\propto r^2$) generally ignored in circular machines is no longer negligible. This driving term may enhance the breathing mode in linacs when the accelerating gradient is high.

2.2. *Linear Paul trap*

The derivation of the LPT Hamiltonian is much easier because the particle motion is non-relativistic. The starting Lagrangian can be written in cylindrical coordinates as

$$L_t = \frac{1}{2} m \left[\dot{r}^2 + (r\dot{\theta})^2 + \dot{z}^2\right] + q(A_r \dot{r} + A_\theta r\dot{\theta} + A_z \dot{z} - \phi), \tag{17}$$

where the dot mark stands for differentiation with respect to the independent variable t. The origin of the coordinate system is fixed at the LPT center, static in the laboratory frame. The z-axis is set along the LPT axis.

The regular LPT only uses the scalar potential to confine charged particles. ϕ is separated into the contribution from the natural space-charge field ($\phi_{\rm sc}$) and that from the artificial electric field ($\phi_{\rm ext}$) for particle confinement. The Hamiltonian derived from Eq. (17) with $A_r = A_\theta = A_z = 0$ and $\phi = \phi_{\rm ext} + \phi_{\rm sc}$ takes the very simple form

$$H_{\rm LPT} = \frac{1}{2m}\left[p_r^2 + \left(\frac{p_\theta}{r}\right)^2 + p_z^2\right] + q\left(\phi_{\rm ext} + \phi_{\rm sc}\right). \tag{18}$$

The transverse confinement of an ion plasma is achieved by an rf quadrupole potential expressed as $\phi_\perp = V_\perp(t)(r/r_0)^2 \cos 2\theta$, where r_0 is the radius of the LPT aperture and $V_\perp(t)$ corresponds to the amplitude of the rf voltages on the four electrode rods placed symmetrically around the z-axis. As described in the next section, the axial confinement potential $\phi_\parallel$ can readily be provided by adding DC or AC bias voltages to electrically isolated quadrupole sections at both ends of the LPT. The linear part is given by $\phi_\parallel = V_\parallel(z^2 - r^2/2)/\ell_z^2$, where $V_\parallel$ is the voltage applied to the end sections and ℓ_z is the characteristic length that depends on the electrode design; ℓ_z can be estimated by solving Maxwell's equations numerically. Substituting the explicit form of $\phi_{\rm ext}$ into Eq. (18), we have

$$H_{\rm LPT} = \frac{1}{2m}\left[p_r^2 + \left(\frac{p_\theta}{r}\right)^2 + p_z^2\right] + \left[qV_\perp(t)\left(\frac{\ell_z}{r_0}\right)^2 \cos 2\theta - \frac{qV_\parallel}{2}\right]\left(\frac{r}{\ell_z}\right)^2 + qV_\parallel\left(\frac{z}{\ell_z}\right)^2 + q\phi_{\rm sc}. \tag{19}$$

The field gradient function $G(z)$ of a DTL is determined by the dimension and arrangement of quadrupole magnets in the drift tubes, which means that it is not highly flexible after the construction of the machine. In contrast, controlling the waveform of the function $V_\perp(t)$ in Eq. (19) is very easy because it has nothing to do with the mechanical structure of the LPT but is simply proportional to the rf voltages on the quadrupole rods. In order to emulate the focusing/defocusing (FODO) lattice adopted in many DTLs around the world, we employ a pulse voltage as illustrated in Fig. 1. The

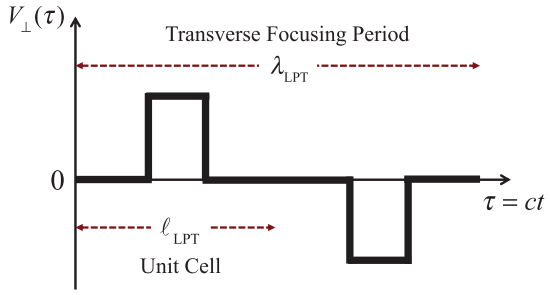

Fig. 1. Radio-frequency waveform of the quadrupole voltage $V_\perp$ emulating the most standard FODO lattice.

cell length in the time domain is equal to $\lambda_{\rm LPT}/2c$, where $\lambda_{\rm LPT}$ is the wavelength of the operating rf field. Note that the transverse focusing period is twice the cell length. When $V_\parallel$ is constant, the phase advance of the axial particle oscillation *per cell* is evaluated from $\sigma_\parallel^2 = 2(\ell_{\rm LPT}/\ell_z)^2(qV_\parallel/mc^2)$, where $\ell_{\rm LPT} \equiv \lambda_{\rm LPT}/2$ corresponds to $\ell_{\rm c}$ in the DTL case. Equation (19) is transformed to

$$\tilde{H}_{\rm LPT} = \frac{1}{2}\left[\tilde{p}_r^2 + \left(\frac{\tilde{p}_\theta}{r}\right)^2 + \tilde{p}_z^2\right] + \left[\frac{qV_\perp(\tau)}{mc^2}\left(\frac{\ell_{\rm LPT}}{r_0}\right)^2\cos 2\theta - \frac{\sigma_\parallel^2}{4}\right]\left(\frac{r}{\ell_{\rm LPT}}\right)^2 + \frac{\sigma_\parallel^2}{2}\left(\frac{z}{\ell_{\rm LPT}}\right)^2 + \frac{q}{mc^2}\phi_{\rm sc} \qquad (20)$$

after scaling the canonical momenta as

$$\tilde{p}_r = \frac{p_r}{mc}, \quad \tilde{p}_\theta = \frac{p_\theta}{mc}, \quad \tilde{p}_z = \frac{p_z}{mc}, \quad \text{and} \quad \tilde{H}_{\rm LPT} = \frac{H_{\rm LPT}}{mc^2}.$$

The independent variable has also been scaled to $\tau = ct$ in Eq. (20). It is now evident that under the linear approximation $\tilde{H}_{\rm LPT}$ has essentially the same form as $\tilde{H}_{\rm DTL}$, including the space-charge potential $\phi_{\rm sc}$ that satisfies the Poisson equation. In either dynamical system, the particle distribution function in phase space obeys the Vlasov equation as long as interparticle Coulomb collisions are negligible. The compact LPT system can, therefore, be used to study diverse space-charge-induced collective phenomena in high-intensity DTLs [3,4].

3. LPT for short-bunch experiment

3.1. Electrode design

At present, three S-POD systems (S-POD I, II, and III) are operating side by side at the Beam Physics Laboratory in Hiroshima for studies of fundamental issues related mostly to transverse beam dynamics. The fourth S-POD system (S-POD IV) is now under construction for short-bunch experiments. All LPTs designed for these systems consist of several (typically, five) independent quadrupole sections electrically isolated from each other so that we can apply different bias voltages to form an axial potential well. The aperture size r_0 has been fixed at 5 mm. The non-linear fields caused within the aperture by the non-hyperbolic surface of the electrodes can be minimized by choosing the proper rod radius ρ [30]. The optimum ratio of ρ to r_0 is 1.15, which gives $\rho = 5.75$ mm in our case. The arrangement of the LPT electrodes for S-POD IV is shown schematically in Fig. 2. Ions are confined in the central region, above which a compact electron gun is placed for the ionization of neutral gas atoms. Separate quadrupole sections of axial length $\ell_{\rm end}$ are set 0.5 mm apart from the

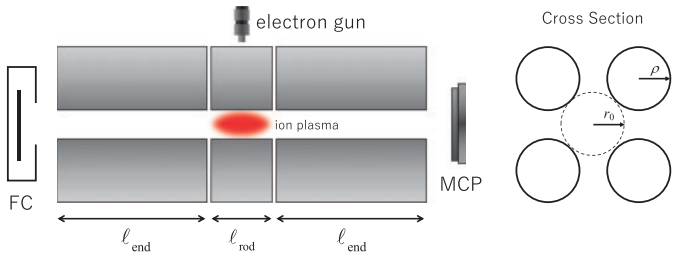

Fig. 2. Schematic drawing of the LPT for short-bunch experiments.

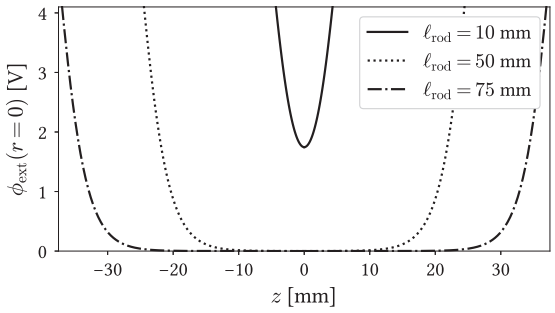

Fig. 3. Potential-well profile on the LPT axis ($r = 0$). The aperture size r_0, i.e. the minimum distance from the axis to the quadrupole rods, is fixed at 5 mm. The diameter of each rod is 11.5 mm. The whole structure consists of three independent quadrupole sections placed 0.5 mm apart, as sketched in Fig. 2. The central section of axial length $\ell_{\rm rod}$ has been grounded while the other two quadrupole sections on each side have an identical bias potential of 10 V. These biased sections are chosen to be sufficiently long ($\ell_{\rm end} = 30$ mm) that the potential profile depends only on $\ell_{\rm rod}$.

central rods. The bias voltage on either of these end sections is eventually dropped to extract ions toward the Faraday-cup (FC) detector or the micro-channel plate (MCP) with a phosphor screen.

A large number of ions are stored in the central quadrupole section of axial length $\ell_{\rm rod}$ for various beam-physics experiments; $\ell_{\rm rod}$ has been chosen to be 50 mm or longer in S-POD I, II, and III. The bias potentials for axial ion confinement are then shielded by the long central rods, which makes the spatial configuration of the plasma bunch more or less like a column rather than an ellipsoid. In order to create an approximately parabolic potential well along the LPT axis for short-bunch experiments, $\ell_{\rm rod}$ must be comparable to the aperture size $2r_0$. Figure 3 shows the potential along the LPT axis ($r = 0$) evaluated with a 3D Maxwell equation solver.

The nominal operating frequency of the LPTs for the S-POD systems is in the MHz range. Since the rf wavelength is far greater than the LPT dimension, we can employ the static field approximation; namely, the rf potential $\phi_{\rm ext}$ can be expressed as the product of two functions, one depending only on time t and the other on the spatial coordinates (r, θ, z). The latter function satisfies Laplace's equation. The results in Fig. 3 are based on the same electrode arrangement as considered in Fig. 2. We have taken three different values of $\ell_{\rm rod}$, while $\ell_{\rm end}$ is fixed at 30 mm. The potential-well profile in the central region becomes almost independent of $\ell_{\rm end}$ once this parameter exceeds a certain threshold. In the present design, where $r_0 = 5$ mm, the threshold is about 15 mm according to a numerical solution of Maxwell's equations. We see that the axial potential profile gets more parabolic as the central electrodes are shortened.

Careful analysis of the aperture field reveals that a proper choice of $\ell_{\rm rod}$ considerably improves the linearity of the external restoring force along the LPT axis. In an ideal LPT with no mechanical

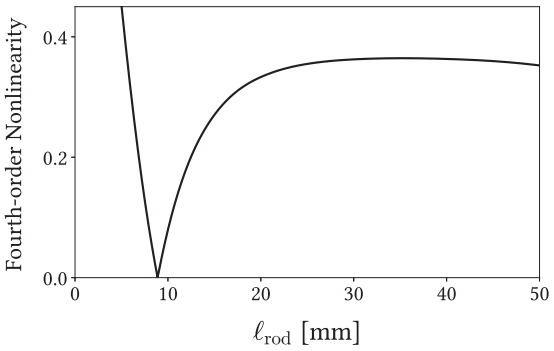

Fig. 4. Strength of the fourth-order field, relative to that of the linear confinement field, along the LPT axis in the absence of electrode misalignments. The mechanical design of the LPT is identical to that assumed in Fig. 3 except that the central-rod length $\ell_{\rm rod}$ is used as a free parameter here.

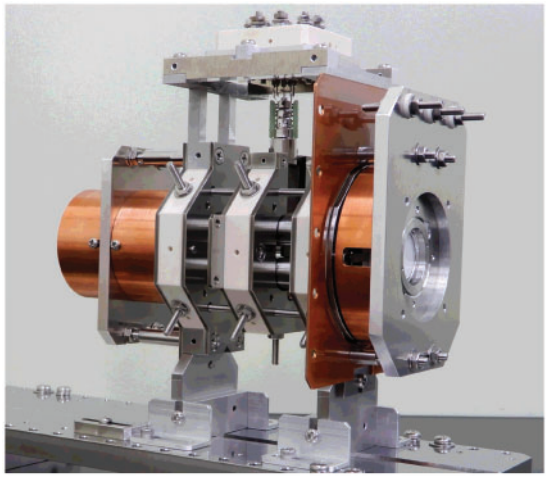

Fig. 5. The LPT constructed for short-bunch experiments in S-POD IV. The mechanical design is based on the electric field analysis described in Sect. 3.1. Some fundamental parameters are the following: $r_0 = 5.0\,$mm, $\rho = 5.75\,$mm, $\ell_{\rm rod} = 8.9\,$mm, and $\ell_{\rm end} = 30.0\,$mm.

errors, the lowest non-linearity expected in the axial confinement potential is the fourth order because of the symmetry of the structure. Expanding the aperture field into multipole components we obtain Fig. 4, which indicates the relative strength of the axial fourth-order field as a function of $\ell_{\rm rod}$. Interestingly, there is a minimum at $\ell_{\rm rod} = 8.9\,$mm. Figure 5 is a picture of the newly constructed LPT for S-POD IV.

3.2. Experimental setup

We have so far trapped $^{40}Ar^{+}$ ions that can easily be produced from neutral Ar gas atoms through the electron bombardment process. The ion species used for S-POD experiments is not essential, as is clear from the Hamiltonian in Eq. (20). The mass and charge state of confined ions are nothing but scaling parameters; if a different ion species is adopted, we change the other parameters correspondingly to maintain the bare phase advances and tune depressions that play a crucial role in intense beam dynamics. In a typical LPT design as described in the previous subsection, i.e. $r_0 = 5\,$mm and a nominal rf frequency in the MHz range, we need the maximum rf amplitude below only a few hundred volts to survey the whole betatron tune space with $^{40}Ar^{+}$ plasmas.

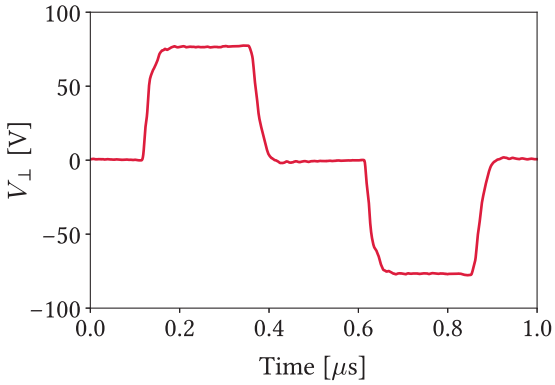

Fig. 6. Example of the pulse voltage generated by the power supply system of S-POD. The pulse height is adjusted to have a bare betatron phase advance of 90° for an $^{40}Ar^{+}$ ion in the absence of the rf defocusing effect. The repetition frequency is set at 1 MHz.

One of the advantages in the tabletop experiment with S-POD is high flexibility and controllability of the AG lattice function, as mentioned above. An extremely wide range of choices is available for the function $V_\perp(\tau)$ in Eq. (20), unlike the function $G(z)$ in Eq. (16) that can only be adjusted within some limited range after the machine is built. Figure 6 shows an example of the rf voltage generated by the S-POD power source to emulate the symmetric FODO lattice. Any ratio of the pulse width to the focusing period (quadrupole filling factor) can be achieved in S-POD [11]. It is possible to provide a variety of pulse waveforms much more complex than the FODO type. The actual rf voltages on the electrodes of the central and end sections are monitored with an oscilloscope to experimentally determine the coefficients of the linear focusing terms in the Hamiltonian to accurately evaluate the betatron and synchrotron phase advances.

Once the axial potential well is switched on, the net phase advances in the transverse directions are reduced due to the defocusing term proportional to $\sigma_\parallel^2$ in Eq. (20). This directly corresponds to the rf defocusing effect in the accelerating gaps of a linac. The axial potential was usually kept static in past S-POD experiments, and therefore unable to be a source of any resonance. The bias voltage $V_\parallel$ is now periodically modulated to excite the synchrotron resonance for the study of high-intensity DTLs. The most typical waveform for $V_\parallel$ is depicted in Fig. 7, where the period is half of the transverse lattice period in Fig. 1. In standard Alvarez DTLs, the transverse AG focusing period is always at least twice as long. Considering the possibility that the synchrotron motion couples with the betatron motion via the strong space-charge potential at high beam density, the true period of the longitudinal driving force may be understood to coincide with the transverse lattice period. In that case, the maximum allowable synchrotron phase advance per cell will be quite limited to ensure the axial beam stability. This is one of the important subjects that can be explored systematically with S-POD.

The characteristic length ℓ_z introduced to define the focusing potential in the axial direction can be estimated on the basis of the numerical data of the aperture field obtained from Maxwell's equations under a proper boundary condition. Assuming the electrode design for the LPT in Fig. 5, the linear coefficient of the multipole field expansion leads to $\ell_z \approx 8.23$ mm. For $^{40}Ar^{+}$ ions confined at the operating frequency of 1 MHz, the phase advance per cell is given by $\sigma_\parallel\,[\mathrm{deg}] \approx 8.54 \times \sqrt{V_\parallel\,[\mathrm{V}]}$ when the axial confinement potential is static (uniform focusing). Only around 100 V turns out to be enough for $V_\parallel$ to cover a typical range of $\sigma_\parallel$ in ordinary DTLs. Provided that the axial focusing force is not static but varies periodically as illustrated in Fig. 7, the use of the smooth approximation

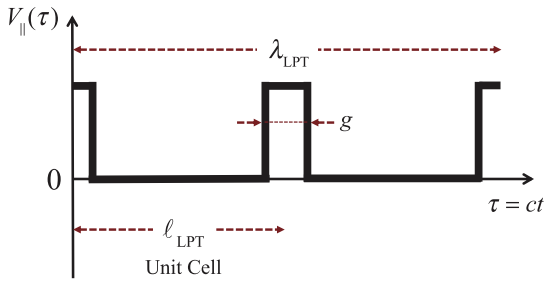

Fig. 7. Radio frequency waveform of the axial confinement voltage $V_\parallel$.

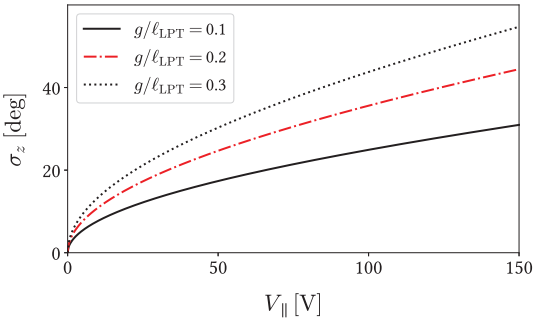

Fig. 8. Synchrotron phase advance per unit cell estimated from Eq. (21). The ion species considered here is $^{40}Ar^+$ confined in an LPT that has the same electrode design as in Fig. 5. We have assumed the pulse waveform shown in Fig. 7. The operating AG frequency for transverse ion focusing (cf. Fig. 1) is set at 1 MHz. The repetition frequency of the axial square pulse is twice as high. Three different form factors have been considered: $g/\ell_{\rm LPT} = 0.1$, 0.2, and 0.3.

gives a handy formula for the synchrotron phase advance:

$$\sigma_z^2 = \mu + \frac{\mu^2}{2}\sum_{n=1}^{\infty}\left(\frac{\xi_n}{n\pi}\right)^2, \tag{21}$$

where we have assumed a square pulse whose width and height are, respectively, g and $V_\parallel$, as in Fig. 7, ξ_n is the pulse form factor defined by $\xi_n = \sin(n\pi g/\ell_{\rm LPT})/(n\pi g/\ell_{\rm LPT})$, and $\mu = \sigma_\parallel^2 \cdot (g/\ell_{\rm LPT})$; σ_z estimated from Eq. (21) is plotted in Fig. 8 as a function of the pulse height $V_\parallel$ for various $g/\ell_{\rm LPT}$ ratios. Equation (21) is used only for a quick estimate of the necessary voltage.

In reality mechanical errors are inevitable, which affects the theoretical estimate of ℓ_z for the ideal LPT structure. This parameter has to be adjusted somehow to an effective value so that we can correctly evaluate the synchrotron phase advance from the direct measurement data of $V_\parallel$. A simple way is to use resonance. We know that single-particle resonances due to imperfection fields occur when the bare tune is close to rational numbers. This common knowledge can be employed to figure out the real size of ℓ_z. We first experimentally locate the positions of resonance-induced ion losses as a function of the bare synchrotron tune calculated with the theoretically expected size of ℓ_z. If the observed ion-loss regions deviate from rational tunes, we modify ℓ_z to shift them to proper positions. This procedure has already been taken in past S-POD experiments to determine the correction factor to r_0. Note that the measurement needs to be done in the low-density regime where the tune shift due to space charge is negligible. A periodic modulation of the potential $V_\parallel$ is also necessary to excite the synchrotron resonance.

4. Concluding remarks

A general Hamiltonian formalism has been constructed to describe the collective behavior of an intense hadron bunch propagating in a standard DTL structure. The Hamiltonian of an ion plasma confined in an LPT is also derived that indicates that these two many-body Coulomb systems are physically equivalent in the regime of interest. This dynamical similarity is the basis of the S-POD apparatus developed at Hiroshima University. S-POD provides us with a local tabletop environment where diverse experimental investigations of fundamental beam dynamics issues can be conducted without the use of large-scale machines. A very compact LPT has been designed and already introduced in S-POD IV for the upcoming tabletop experiment. S-POD IV is intended to clarify the stability of intense short bunches in hadron linacs, while past studies with S-POD I, II, and III have focused on the transverse beam dynamics in circular machines [5–12].

In hadron linacs the synchrotron tune can be comparable to the betatron tune, unlike in regular rings. A clear understanding of the interplay between betatron and synchrotron motions is thus more important. For instance, the rf defocusing term in the Hamiltonian originating from the axial focusing potential should have a non-negligible impact on the transverse beam stability. It not only reduces the effective focusing force in the transverse directions but also yields rather strong periodic perturbation to the betatron motion at high accelerating efficiency. Hofmann and Boine-Frankenheim have argued that the longitudinal stability may be treated independently of the transverse stability and, therefore, not limited by the periodicity of the magnetic AG lattice [31]. The defocusing effect at every accelerating gap is, however, axisymmetric, which can drive the breathing oscillation that modulates the transverse charge density at the frequency corresponding to the rf period. If the space-charge coupling is strong, the transverse motion will "see" the longitudinal focusing period and vice versa. A recent theoretical study by Qiang indicates a sort of synchro-betatron coupling effect in high-intensity accelerators [32]. Employing a 3D envelope model, he pointed out the possibility of beam instability that occurs at the betatron phase advance below 90° when the synchrotron phase advance exceeds 90°.

Another interesting subject we might consider is the problem of resonance crossing. Lee et al. have stated that the systematic space-charge resonances of the *fourth* and even *sixth* orders may cause substantial emittance growth when they are crossed in a fixed-field AG accelerator of the non-scaling type [33,34]. We can easily move the operating point of an LPT at arbitrary speed by ramping the rf amplitude. The effect of resonance crossing has already been studied in detail with S-POD assuming a relatively long bunch without the synchrotron resonance [6,9]. The use of S-POD IV with the new LPT makes it possible to extend this previous study to a short-bunch situation with a longitudinal periodic driving force switched on. According to the envelope theory by Qiang, the 90° stop band due to the linear coherent instability might be crossed without serious emittance growth in a high-intensity linac with a reasonable accelerating gradient [35]. All these issues of practical importance in hadron linacs can be explored systematically with S-POD IV.

The initial phase-space density of an ion plasma produced in an LPT has so far been controlled by changing the neutral gas pressure and electron-beam current from the *e*-gun. The lowest tune depression achievable with this simple procedure is limited to about 0.8.[3] The use of a laser-coolable ion species greatly extends the beam-density range we can survey. The best candidate for the present

[3] The *tune depression* is usually defined as the ratio of the space-charge-depressed tune to the bare tune. It therefore decreases as the beam density becomes higher. At low density it is close to unity.

S-POD system is $^{40}Ca^{+}$ that can be cooled with inexpensive semiconductor lasers. Since the charge-to-mass ratio is identical to that of $^{40}Ar^{+}$, we do not have to develop new AC and DC power sources. S-POD I and II are already equipped with a Doppler laser cooler for $^{40}Ca^{+}$. As the Doppler limit is close to absolute zero, we can reach the ultimate space-charge limit where the betatron and synchrotron oscillations of individual particles are completely suppressed; in other words, the tune depression is zero in all three dimensions. By controlling the cooling time and laser detuning, it is probably possible to develop a large emittance imbalance (temperature anisotropy) between the axial and transverse degrees of freedom. We may then be able to explore the role of *equipartitioning* in beam stability [25,27,36], e.g. whether an initially anisotropic beam may be less stable in the space-charge-dominated regime [37]. This is an important future issue that could be studied with the new LPT. Furthermore, laser-induced fluorescence diagnostics is usable for high-precision profile measurement and even to probe the ion distribution in phase space. Ca is, however, solid at room temperature, unlike Ar, which makes the plasma production process somewhat more cumbersome. A recent experimental study with S-POD I shows that a large number of $^{40}Ca^{+}$ ions can be accumulated in an LPT by optimizing the axial potential profile [38].

Acknowledgements

This work is supported in part by Japan Society for the Promotion of Science (JSPS) KAKENHI Grant Number 18H03472.

References

[1] R. Takai, H. Enokizono, K. Ito, Y. Mizuno, K. Okabe, and H. Okamoto, Jpn. J. Appl. Phys. **45**, 5332 (2006).
[2] R. Takai, K. Ito, Y. Iwashita, H. Okamoto, S. Taniguchi, and Y. Tomita, Nucl. Instrum. Meth. A **532**, 508 (2004).
[3] H. Okamoto and H. Tanaka, Nucl. Instrum. Meth. A **437**, 178 (1999).
[4] H. Okamoto, Y. Wada, and R. Takai, Nucl. Instrum. Meth. A **485**, 244 (2002).
[5] S. Ohtsubo, M. Fujioka, H. Higaki, K. Ito, H. Okamoto, H. Sugimoto, and S. M. Lund, Phys. Rev. ST Accel. Beams **13**, 044201 (2010).
[6] H. Takeuchi, K. Fukushima, K. Ito, K. Moriya, H. Okamoto, and H. Sugimoto, Phys. Rev. ST Accel. Beams **15**, 074201 (2012).
[7] H. Okamoto, M. Endo, K. Fukushima, H. Higaki, K. Ito, K. Moriya, S. Yamaguchi, and S. M. Lund, Nucl. Instrum. Meth. A **733**, 119 (2014).
[8] K. Fukushima, K. Ito, H. Okamoto, S. Yamaguchi, K. Moriya, H. Higaki, T. Okano, and S. M. Lund, Nucl. Instrum. Meth. A **733**, 18 (2014).
[9] K. Moriya, K. Fukushima, K. Ito, T. Okano, H. Okamoto, S. L. Sheehy, D. J. Kelliher, S. Machida, and C. R. Prior, Phys. Rev. ST Accel. Beams **18**, 034001 (2015).
[10] K. Moriya, M. Ota, K. Fukushima, M. Yamaguchi, K. Ito, and H. Okamoto, Phys. Rev. Accel. Beams **19**, 114201 (2016).
[11] K. Ito, H. Okamoto, Y. Tokashiki, and K. Fukushima, Phys. Rev. Accel. Beams **20**, 064201 (2017).
[12] K. Ito, M. Matsuba, and H. Okamoto, Prog. Theor. Exp. Phys. **2018**, 023G01 (2018).
[13] E. P. Gilson, R. C. Davidson, P. C. Efthimion, and R. Majeski, Phys. Rev. Lett. **92**, 155002 (2004); **93**, 239902 (2004) [erratum].
[14] M. Chung, E. P. Gilson, R. C. Davidson, P. C. Efthimion, and R. Majeski, Phys. Rev. Lett. **102**, 145003 (2009).
[15] E. P. Gilson, R. C. Davidson, M. Dorf, P. C. Efthimion, R. Majeski, M. Chung, M. S. Gutierrez, and A. N. Kabcenell, Phys. Plasmas **17**, 056707 (2010).
[16] S. Sheehy, D. Kelliher, S. Machida, C. Plostinar, and C. Prior, in *Proc. 7th Int. Particle Accelerator Conf. (IPAC2016), Busan, Korea*, (JACoW, Geneva, 2016), WEPOY048, p. 3104.
[17] S. L. Sheehy, E. J. Carr, L. K. Martin, K. Budzik, D. J. Kelliher, S. Machida, and C. R. Prior, J. Phy.: Conf. Ser. **874**, 012067 (2017).

[18] C. R. Prior, in *Proc. 57th ICFA Advanced Beam Dynamics Workshop on High-Intensity and High-Brightness Hadron Beams, Malmö, Sweden*, (JACoW, Geneva, 2016), WEAM6X01, p. 379.
[19] P. K. Ghosh, *Ion Traps* (Oxford Science, Oxford, 1995).
[20] L. Alvarez, Phys. Rev. **70**, 799 (1946).
[21] J. P. Blewett, Phys. Rev. **88**, 1197 (1952).
[22] L. Alvarez, H. Bradner, J. V. Franck, H. Gordon, J. Donald Gow, L. C. Marshall, F. Oppenheimer, W. K. H. Panofsky, C. Richman, and J. R. Woodyard, Rev. Sci. Instrum. **26**, 111 (1955).
[23] L. Smith and R. L. Gluckstern, Rev. Sci. Instrum. **26**, 220 (1955).
[24] P. M. Lapostolle, *Proton Linear Accelerators: A Theoretical and Historical Introduction*, Los Alamos Report LA-11601-MS (1989).
[25] T. P. Wangler, *RF Linear Accelerators* (John Wiley & Sons, New York, 1998) and references therein.
[26] I. M. Kapchinskiy, *Theory of Resonance Linear Accelerators* (Harwood, Switzerland, 1985).
[27] M. Reiser, *Theory and Design of Charged Particle Beams* (Wiley, New York, 2008) and references therein.
[28] R. D. Ryne, Los Alamos Report No. LA-UR-95-391, available at https://arxiv.org/pdf/acc-phys/9502001.pdf.
[29] Y. K. Batygin, in *Proc. 4th Int. Particle Accelerator Conf. (IPAC2013), Shanghai, China*, (JACoW, Geneva, 2013), TUPWA067, p. 1859.
[30] D. R. Denison, J. Vacuum Sci. Techol. **8**, 266 (1971).
[31] I. Hofmann and O. Boine-Frankenheim, Phys. Rev. Lett. **118**, 114803 (2017).
[32] J. Qiang, Phys. Rev. Accel. Beams **21**, 034201 (2018).
[33] S. Y. Lee, G. Franchetti, I. Hofmann, F. Wang, and L. Yang, New J. Phys. **8**, 291 (2006).
[34] S. Y. Lee, Phys. Rev. Lett. **97**, 104801 (2006).
[35] J. Qiang, Phys. Rev. Accel. Beams **21**, 114201 (2018).
[36] R. A. Jameson, IEEE Trans. Nucl. Sci. **28**, 2408 (1981).
[37] I. Hofmann, Phys. Rev. E **57**, 4713 (1998).
[38] K. Ito, T. Masuda, H. Higaki, and H. Okamoto, in *Proc. 10th Int. Particle Accelerator Conf. (IPAC2019), Melbourne, Australia*, (JACoW, Geneva, 2019), WEPTS019, in press.